PROCEEDINGS OF SCIENCE

Electron Acceleration at Rippled Low Mach Number Shocks in Merging Galaxy Clusters

Oleh Kobzar[a], **Jacek Niemiec**[*a], **Takanobu Amano**[b], **Masahiro Hoshino**[b], **Shuichi Matsukiyo**[c], **Yosuke Matsumoto**[d], **Martin Pohl**[e,f]

[a] *Institute of Nuclear Physics Polish Academy of Sciences, PL-31342 Krakow, Poland*
[b] *Department of Earth and Planetary Science, the University of Tokyo, 7-3-1 Hongo, Bunkyo-ku, Tokyo 113-0033, Japan*
[c] *Faculty of Engineering Sciences, Kyushu University, 6-1 Kasuga-Koen, Kasuga, Fukuoka, 816-8580, Japan*
[d] *Department of Physics, Chiba University, 1-33 Yayoi-cho, Inage-ku, Chiba 263-8522, Japan*
[e] *DESY, 15738 Zeuthen, Germany*
[f] *Institute of Physics and Astronomy, University of Potsdam, 14476 Potsdam, Germany*
E-mail: Jacek.Niemiec@ifj.edu.pl

Shock waves are ubiquitous in cosmic plasmas wherein they accelerate particles. In particular, X-ray and radio observations of so-called radio relics indicate electron acceleration at large-scale merger shocks in galaxy clusters. These shocks are also candidate sites for ultra-high-energy cosmic ray production. Merger shocks have low Mach numbers and propagate in hot plasmas with plasma beta $\beta \gg 1$. Particle energization and especially electron injection mechanisms are poorly understood in such conditions. Recent studies show that shock drift acceleration (SDA) accompanied by particle-wave interactions can provide electron acceleration, albeit a multi-scale shock structure in the form of ion-scale shock rippling may significantly alter the injection mechanisms. Here we study the effects of the shock rippling with large-scale 2D PIC simulations of low Mach number cluster shocks. We find that the electron acceleration rate increases considerably after the appearance of wave-rippling modes. The main acceleration process is stochastic SDA, in which electrons are confined in the shock transition region by pitch-angle scattering off magnetic turbulence and gain energy from motional electric field. The presence of multi-scale turbulence in the shock is essential for particle energization. Wide-energy non-thermal electron distributions are formed both upstream and downstream of the shock. We show for the first time that the downstream electron spectrum has a power-law form with index $p = 2.4$, in agreement with observations.

36th International Cosmic Ray Conference -ICRC2019-
July 24th - August 1st, 2019
Madison, WI, U.S.A.

*Speaker.

PoS(ICRC2019)368

1. Introduction

Merger shocks at the outskirts of galaxy clusters show radio synchrotron emission from relativistic electrons, so-called radio relics [1]. Connection of radio relics with shocks suggests electron production via diffusive shock acceleration (DSA, or 1st-order Fermi) process. Observations indicate that merger shocks are weak, i.e., their sonic Mach numbers are very low, $M_{\rm s} \lesssim 4$, though probably still supercritical. They propagate in hot intracluster medium (ICM), in which plasma beta – a ratio of thermal to magnetic pressure in the pre-shock plasma – is high ($\beta \gg 1$). Particle acceleration, and especially electron injection mechanisms, are poorly understood in this regime.

Electron acceleration at low Mach number high β shocks has recently been studied with one- and two-dimensional (1D and 2D) fully kinetic particle-in-cell (PIC) simulations. First 1D simulations [3] and later 2D simulations [2] showed that in such shocks electrons can be efficiently energized via shock drift acceleration (SDA), in which particles are accelerated via motional electric field while drifting along the shock surface due to magnetic field gradient at the shock. In high plasma β conditions and at *subluminal* shocks some SDA-accelerated electrons are reflected from the shock and form non-equilibrium velocity distribution in the foreshock region that leads to instabilities which generate waves. It was proposed in [3] that electrons can be scattered on these waves back towards the shock to experience further acceleration. This scenario has been confirmed in 2D simulations [4, 5] that demonstrated that upstream scattering allows for repeated SDA cycles, similar to a sustained 1st-order Fermi process. The upstream waves have been identified with the oblique mode of the electron firehose instability (EFI), driven by the electron temperature anisotropy caused by electrons reflected from the shock and streaming along the mean magnetic field. Systematic investigations indicated that such mechanisms of wave generation and electron scattering work for parameters in galaxy clusters in particular in high beta plasmas, $\beta \gtrsim 20$ [5]. For shock obliquities that allow large fractions of reflected electrons and thus strong temperature anisotropy, non-thermal power-law tails with slope $p = 2.4$ in the energy spectra ($dn/d\gamma \propto \gamma^{-p}$) were found, giving radio synchrotron index of -0.7, compatible with observations. However, such spectra were shown to be formed only in the *upstream* region of the shock, and downstream spectra were still close to thermal distributions. Most recent similar studies show that such electron preacceleration occurs only in shocks above a so-called "EFI critical Mach number", $M^*_{\rm ef} \approx 2.3$, and shocks with $M_{\rm s} \lesssim 2.3$ cannot accelerate electrons [6]. On the other hand, at supercritical shocks with $M_{\rm s} \gtrsim M^*_{\rm ef}$ electrons may not reach a sufficiently high energy to be injected into DSA, because EFI was observed to saturate and did not generate long-wavelength modes.

The studies reported above used simulation boxes of small transverse size that do not account for the multi-scale shock structure that includes ion-scale fluctuations in the form of the shock surface corrugations. The first such attempt has recently been reported in large-scale 2D simulations of shocks with $\beta = 3$ [7], that were earlier studied with 1D simulations [3] and showed efficient SDA. Shock rippling was observed to appear in the simulations, the origin of which is considered to be due to downstream temperature anisotropy of ions provided by shock-reflected ions that were convected back downstream. In this case Alfvén ion cyclotron (AIC) instability can be triggered. The rippling was shown to form local regions of weaker magnetic field along the shock surface, and electrons undergoing SDA at the overshoot are transmitted downstream and are not reflected upstream. Almost all electrons encounter the weak field region during their SDA interaction with

the shock. However, some non-thermal electrons can still be found at the shock. This population was energized through wave-particle interactions in the shock transition.

With growing plasma beta, the temperature anisotropy becomes smaller, the growth rate of the AIC instability decreases and the rippling modes have larger wavelengths. It was estimated that for parameters used in [4, 5, 6] in simulations with $\beta = 20$ or higher, the ripple wavelength is much larger than the transverse box size they used, so that the modes could not be resolved. On the other hand, at plasma β close to that used in [7], a sustained Fermi-like process may be inhibited on account of the strong magnetic pressure that suppresses the growth of the EFI, even though electron reflection via SDA can be efficient. The effects of the shock rippling thus need to be investigated in the regime in which the Fermi-like acceleration can operate. This is the aim of our present study with large-scale 2D PIC simulations. Preliminary results are reported here.

2. Simulation setup

Our simulation setup is shown in Figure 1. Electron-ion plasma beam is injected at the right side of the simulation box to flow with a bulk velocity v_0 in the negative x-direction. Upon reflection off the conductive wall, the beam starts to interact with the incoming plasma forming the shock that propagates with velocity $v_{\rm sh}$. The simulation box is placed in the $x-y$ plane with open right x-boundary and periodic boundary conditions in the y-direction. The injected plasma carries a large-scale uniform magnetic field, $\boldsymbol{B}_0$, that lies in the simulation plane at the angle $\theta_{\rm Bn} = 75^{\rm o}$ relative to the shock normal. We thus consider a quasi-perpendicular and *subluminal* shock (for our parameters the critical superluminality angle is $\theta_{\rm Bn,crit} \simeq 81.4^{\rm o}$). With the magnetic field a motional electric field $\boldsymbol{E} = -[\boldsymbol{v}_0 \times \boldsymbol{B}_0]$ is also initialized and has non-zero out-of-plane component, E_z.

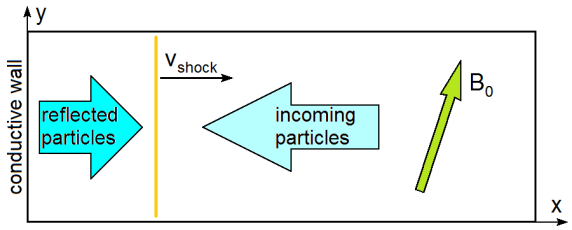

Figure 1: Illustration of the simulation setup. Note that motional electric field $\boldsymbol{E} = -[\boldsymbol{v}_0 \times \boldsymbol{B}_0]$ is directed out of the simulation plane, in the z-direction.

The simulation parameters have been chosen to represent physical conditions at ICM shocks. The bulk flow velocity is $v_0 = 0.1\,c$, where c is the speed of light. The temperature of electrons and ions is initially $T_{\rm e} = T_{\rm i} \approx 5 \cdot 10^8\,{\rm K} = 43\,{\rm keV}/k_{\rm B}$. With this choice the sonic Mach number of the shock measured in the upstream rest frame is $M_{\rm s} \equiv v_{\rm sh}/c_{\rm s} = 3$, where the sound speed $c_{\rm s} = \sqrt{2\Gamma k_{\rm B} T_{\rm i}/m_{\rm i}}$, and Γ is the adiabatic index. Total plasma beta $\beta = 5$ ($\beta_{\rm e} = \beta_{\rm i} = 2.5$). Although this value is lower than β assumed in simulations in which EFI is strongly excited [4, 6], it is a necessary compromise to fit the ion-scale rippling modes in the simulation box and at the same time allow to follow the long-time development of the system under available computing resources. We apply a reduced ion-to-electron mass ratio $m_{\rm i}/m_{\rm e} = 100$. The Alfvénic Mach number of our shock is $M_{\rm A} = v_{\rm sh}/v_{\rm A} \simeq 6.1$, where $v_{\rm A} = B_0/\sqrt{\mu_0(N_e m_e + N_i m_i)}$ is the Alfvén velocity (μ_0 is the vacuum permeability and N_i and N_e are the upstream ion and electron number densities).

The simulation has been performed with 20 particles per cell per particle species. We use $\lambda_{\rm se} \equiv c/\omega_{\rm pe} = 15$ cells, where $\lambda_{\rm se}$ is the electron skin depth and $\omega_{\rm pe} = \sqrt{e^2 N_e/\varepsilon_0 m_{\rm e}}$ is the electron plasma frequency (with e the electron charge and ε_0 the vacuum permittivity). The ion skin depth, $\lambda_{\rm si} = \sqrt{m_{\rm i}/m_{\rm e}}\lambda_{\rm se}$, is our unit of length. The time-step is $\delta t = 1/30\,\omega_{\rm pe}^{-1}$. The ion gyration time-scale is $\Omega_{\rm i}^{-1} = 1.225\cdot 10^4\,\delta t$, where $\Omega_{\rm i} = eB_0/m_{\rm i}$ is the upstream ion gyrofrequency. The transverse size of the simulation box is fixed to $L_y = 320\,\lambda_{\rm se} = 32\,\lambda_{\rm si}$, and its length grows with simulation time up to $L_x \approx 4000\,\lambda_{\rm se} = 400\,\lambda_{\rm si}$. The maximum simulation time $t_{\rm max}\Omega_{\rm i} \simeq 79$.

3. Results

3.1 Shock structure

Figure 2 shows the shock structure at times $t\Omega_{\rm i} = 18$ and $t\Omega_{\rm i} = 35$. The shock at $t\Omega_{\rm i} = 18$ is located at $x/\lambda_{\rm si} \approx 43$. Its structure is laminar and shows an overshoot-undershoot system, typical of quasi-perpendicular shocks. By the time $t\Omega_{\rm i} \approx 25$, the rippling mode appears in the shock overshoot and at $t\Omega_{\rm i} \approx 35$ (Fig. 2 *right*) it already assumes a well-developed form with wavelength $\lambda_{\rm rippl} = 16\,\lambda_{\rm si}$, that is consistent with the wavelength of $\sim 18\,\lambda_{\rm si}$ derived from the linear analysis under the assumption that the rippling results from the AIC instability. Since the ion temperature anisotropy persists throughout the shock transition region, also the structure of the second overshoot (located at $x/\lambda_{\rm si} \approx 31$ in Fig. 2 *left*) is corrugated. Ripples in this region emerge earlier and with shorter wavelengths than the ripple mode in the overshoot, and with time they cascade into smaller wavenumber modes. The electromagnetic structure of the transition region past the first overshoot suggests that the modes in this region are related to AIC and/or mirror instabilities. The magnetic field maps also show small-scale waves in the first and second overshoot. They have B_x and B_z field components and propagate upward along the compressed mean magnetic field. We identify these waves with right-hand circularly-polarized whistlers excited by the ion temperature anisotropy.

Figure 2b shows the presence of weak magnetic waves upstream of the overshoot (for $x/\lambda_{\rm si} \gtrsim 80$), that have a wavevector, $\boldsymbol{k}$, at the angle $\theta_{\rm Bk} \approx 70^{\rm o}$ to $\boldsymbol{B}_0$. These waves can be identified with

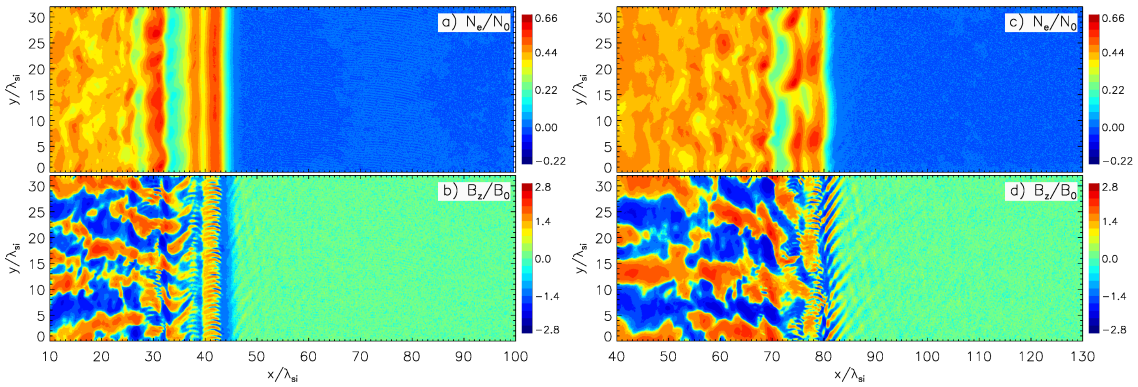

Figure 2: Distribution of the electron number density $N_{\rm e}/N_0$ (*top panels, (a)* and *(c)*) and the structure of B_z/B_0 magnetic field component (*bottom panels, (b)* and *(d)*) at time $t\Omega_{\rm i} = 18$ (*left*) and $t\Omega_{\rm i} = 35$ (*right*). Logarithmic scaling is applied to density maps. The scaling for magnetic fields is also logarithmic, but sign-preserving ($\mathrm{sgn}(B_z)\cdot\{2+\log[\max(|B_z|/B_0, 10^{-2})]\}$), so that field amplitudes below $10^{-2}B_0$ are not resolved.

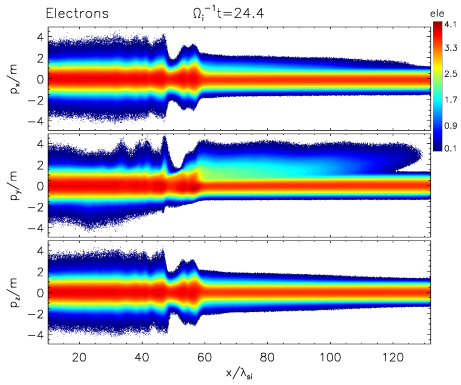

Figure 3: Phase-space distribution of electrons at time $t\Omega_i t = 24.2$, averaged over the transverse box direction (from top to bottom: p_x/m_e, p_y/m_e, and p_z/m_e). The shock is located at $x/\lambda_{si} \approx 57$.

the oblique mode of the EFI, driven by the electron temperature anisotropy provided by electrons reflected from the shock in the SDA process. Low amplitudes of these waves at this stage of the system evolution are consistent with the theoretical expectation that electron reflection is not efficient in conditions that have $v_{th,e} \lesssim v_t$, where $v_t = v_{sh}^{up}/\cos\theta_{Bn}$ is de Hoffman-Teller velocity [4]. In our simulation we have $v_t \approx 1.5\, v_{th,e}$. Nevertheless, as one can see in Figure 2d, the amplitudes of the EFI modes are strongly amplified upon the emergence of the shock ripples, and their structure is modulated with the wavelength of the overshoot corrugations. This demonstrates that the shock ripples locally enhance the electron reflection rate along the shock surface, enabling more efficient EFI wave generation. This might occur because conditions with $v_{th,e} \gtrsim v_t$ are formed locally along the shock and/or ripples enhance electron reflection above a certain critical electron energy. It is consistent with the previous work [7] in which electron reflection is suppressed by the ripples. In [7] the upstream beta ($\beta = 3$) is relatively low so that there may be no electrons above the critical energy. The electron phase-space distribution at the time of the appearance of the ripples ($t\Omega_i = 24.2$) is shown in Figure 3. A population of reflected electrons that propagate away from the shock along the upstream magnetic field lines is clearly visible in p_y and p_x momenta.

In summary, the subluminal low Mach number shock in the regime of high plasma beta analysed here shows strongly turbulent and dynamic structure of the transition region with broad-band spectrum of field and density perturbations. This multi-scale turbulent structure of the shock is of profound importance for the electron acceleration processes, as discussed below.

3.2 Electron acceleration

Figures 4 and 5 show the time evolution of electron spectra upstream and downstream of the shock, respectively. The acceleration process operates from the early laminar shock stage, and upstream spectra are consistent with SDA predictions at this phase (*magenta* line in Fig. 4a). However, the acceleration rate (Fig. 4b) increases considerably after the appearance of rippling at $t\Omega_i \approx 25$, contrary to what was observed in [7]. In effect, electron spectra are formed in a wide-energy range, and the maximum Lorentz factor reaches $\gamma_{max} \approx 60$. This value is much larger than is needed for injection to DSA, $\gamma_{inj} \approx 25$, estimated under assumption that the injection momentum $p_{inj} \sim 3p_{th,i}$ [6]. The fraction of supra-thermal particles reaches 5%, and $\sim 40\%$ of the energy

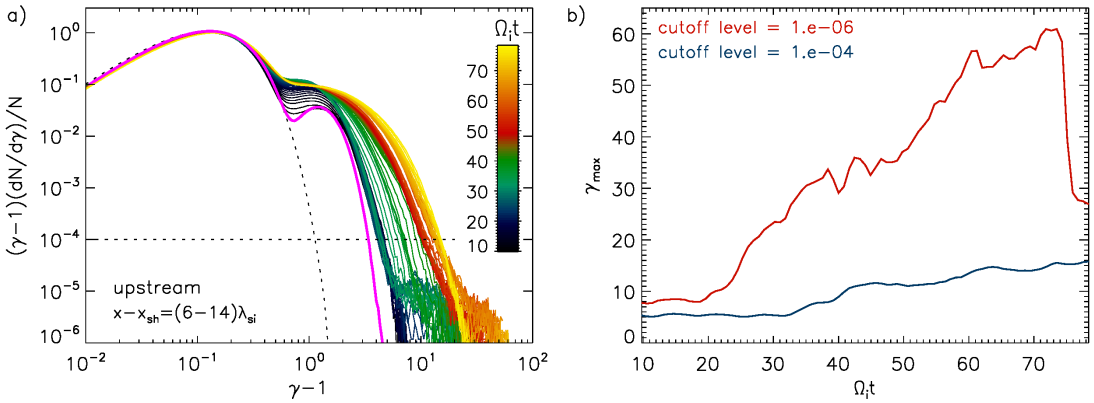

Figure 4: *Panel (a)*: Color-coded evolution of the electron energy spectra upstream of the shock. Magenta line shows theoretical prediction of SDA. Maxwellian fit to low-energy part of the spectra is shown with a dotted line. *Panel (b)*: Evolution of $\gamma_{\rm max}$ chosen at different cutoff levels of the spectra in Fig. 4a (bottom axis and horizontal dotted line at 10^{-4}).

density is deposited in energetic electrons. Here, for the first time we demonstrate the formation of extended power-law spectra downstream of the shock, with spectral index $p \simeq 2.4$, in agreement with observations (Fig. 5). The downstream spectrum is approximately stable in our simulation. The supra-thermal tail contains 0.12% of the particles and 1% of the downstream energy density.

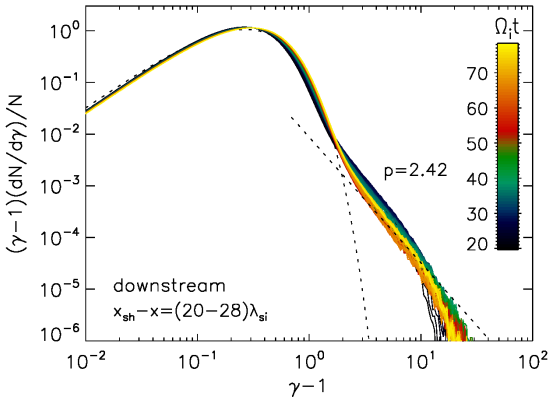

Figure 5: Evolution of electron energy spectra downstream of the shock. Power-law fit with index $p = 2.42$ to the supra-thermal component is shown with dotted line.

Typical trajectories of accelerated particles are shown in Figure 6. Most particles gain energies during a single interaction with the shock. However, they typically do not undergo SDA, for which the acceleration time ($\sim \Omega_{\rm i}^{-1}$) is much shorter than for the majority of particles observed in the simulation. Closer inspection of two particle orbits in Figure 7 shows that, unlike for SDA, most accelerations are associated with an increase in perpendicular particle momentum, in between which strong pitch-angle scattering occurs, visible as arcs in $p_\parallel - p_\perp$ momentum plots. At the same time, the energy gain is achieved mostly through the drift along the motional electric field, $\Delta\gamma_{\rm drift} = (-e/m_{\rm e}c^2)\int E_z\,dz$, as in SDA (compare *red* and *blue* lines in top panel of Fig. 7). We therefore identify the acceleration process with stochastic shock drift acceleration (SSDA), re-

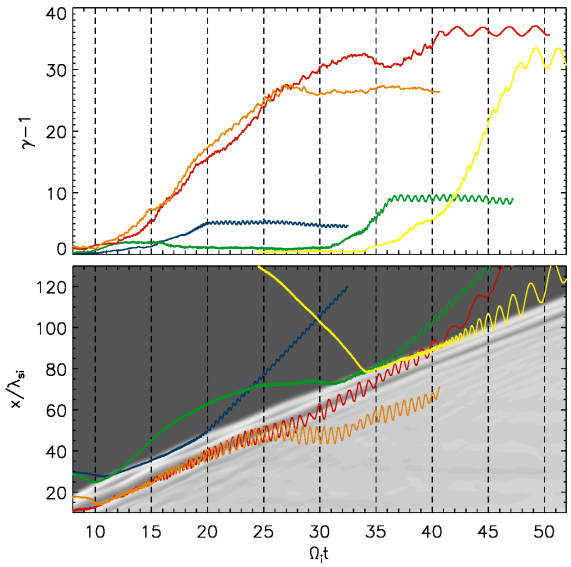

Figure 6: Typical trajectories of accelerated particles and their energy evolution.

cently described in [8]. In this process electrons are confined in the shock transition region by stochastic pitch-angle scattering off magnetic turbulence and gain energy through SDA. Longer particle confinement increases energy gains and enables more efficient acceleration.

The presence of multi-scale turbulence in the shock is essential for particle energization. Acceleration can start with resonant interactions with short-scale whistlers (*blue* and *yellow* particles in Fig. 6) or medium-scale ripples in the second overshoot (*red* and *orange*). In the latter case, the waves pitch-angle scatter electrons and confine them in between the undershoot and overshoot region, where they tap the energy of a weak motional field that persist there. Particles that are energized there are either picked-up from downstream population (*red*) or have been first transmitted downstream (*orange*). In any case the acceleration process can continue once electrons escape back toward the shock surface and further interact resonantly with longer-wave and overdense ripples in the overshoot, that results in exceedingly high electron energies (*red* and *yellow* particles). Highly accelerated electrons are frequently observed to escape upstream at an enhanced rate compared to the laminar stage. EFI-generated waves are then amplified providing additional particle confinement. However, the process of multiple-cycle SDA [4] is not common, and upstream scattering of SDA-reflected particles is typically followed by an SSDA event (*green*). Note that some electrons accelerated in the second overshoot-undershoot region escape downstream (*orange*). The downstream supra-thermal population results from SSDA and is formed much earlier than any substantial number of upstream-accelerated electrons can be advected past the shock.

4. Summary

Kinetic modeling of particle acceleration at low Mach number shocks in high-beta plasmas requires inclusion of multi-dimensional and large-scale effects. For parameters analysed in this work we find the presence of multi-scale turbulence, including ion-scale shock rippling modes,

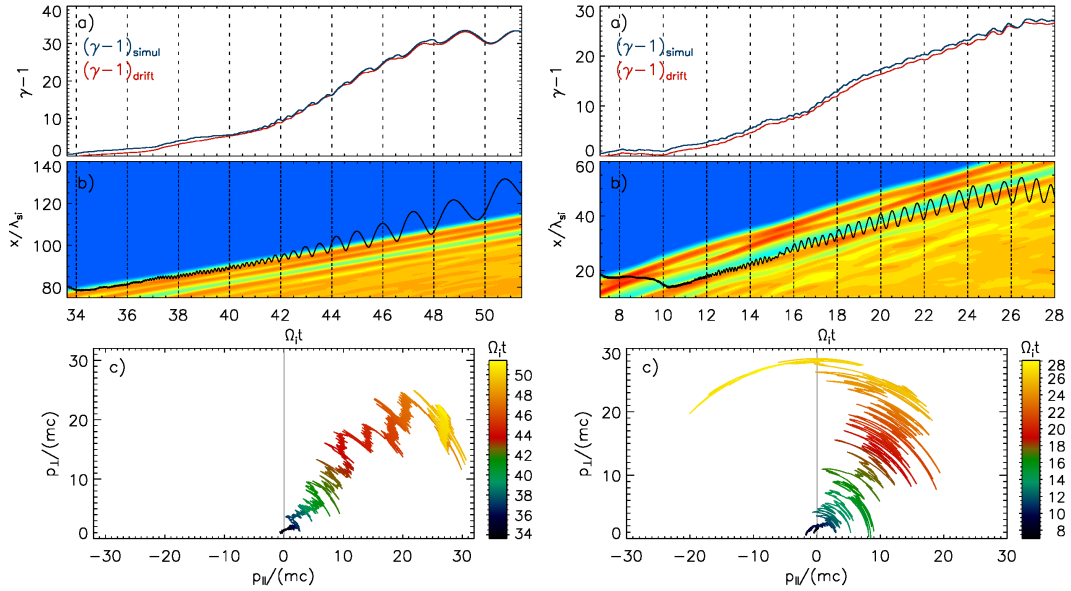

Figure 7: Trajectories of two particles shown in Figure 6 with yellow (*left*) and orange (*right*) lines. From top to bottom panels show time evolution of energy, trajectory with respect to the shock and in $p_\parallel - p_\perp$ momentum space.

to be critical for efficient electron acceleration. Electron injection proceeds mainly through the stochastic SDA process, but the effects of multi-SDA cycles are also observed. Acceleration to very high energies occurs that should lead to electron injection to DSA in the presence of long-wave (MHD) upstream turbulence.

Acknowledgments

The work of O.K. and J.N. has been supported supported by Narodowe Centrum Nauki through research project DEC-2013/10/E/ST9/00662. This work was also supported by JSPS-PAN Bilateral Joint Research Project Grant Number 180500000671. Numerical simulations have been performed on the Prometheus system at ACC Cyfronet AGH and also on resources provided by The North-German Supercomputing Alliance (HLRN) under projects bbp00003 and bbp00014.

References

[1] Brunetti, G., & Jones, T. W. 2014, Int. J. Mod. Phys. D, 23, 1430007-98

[2] Park, J., Workman, J. C., Blackman, E. G., Ren, C., & Siller, R. 2012, Phys. Plasmas, 19, 062904

[3] Matsukiyo, S., Ohira, Y.,Yamazaki, R., & Umeda, T. 2011, ApJ, 742, 47

[4] Guo, X., Sironi, L., & Narayan, R. 2014, ApJ, 794, 153

[5] Guo, X., Sironi, L., & Narayan, R. 2014, ApJ, 797, 47

[6] Kang, H., Ryu, D., & Ha, J.-H. 2019, ApJ, 876, 79

[7] Matsukiyo, S., & Matsumoto, Y. 2015, Journal of Physics Conference Series, 642, 012017

[8] Katou, T., & Amano, T. 2019, ApJ, 874, 119